Part One

Introduction

1

Introduction

1.1 Introduction

For a long time, voltage-type sources such as storage battery, AC grid, and output-voltage-regulated converters have dominated as an input source for power electronic converters [1,2]. These sources are usually referred to as rigid sources, since the load has limited influence on their operating voltage. Both awareness on the depletion of fossil fuel reserves and their impact on the observed climate changes have accelerated the utilization of renewable energy sources, for example, wind and solar [3]. Effective large-scale utilization of these energy sources requires the use of grid-interfaced power electronic converters [4,5]. It has been recently concluded [6,7] that the power electronic converters used in the photovoltaic (PV) systems are essentially current-sourced converters because of the current-source properties of PV generator [8,9] forced by the input-side voltage feedback control [10,11]. At open loop, the static and dynamic properties of the integrating converter are determined by the operating region of the PV generator. The same also applies for the converters in wind energy systems. Another example of a perfect current source is superconducting magnetic energy storage (SMES) system, where a very large inductor serves as the energy storage element [12,13]. Even though the properties of the mentioned sources are already well known [14,15], they are still typically considered as voltage sources when designing the interfacing converter power stages [16,17] or analyzing their underlying dynamics [18–21] despite their current-type properties. The analysis method is usually justified by Norton/Thevenin transformation [20].

The existence of two different input source types implies that two different families of power electronic converters shall also exist, where the converters shall be referred to as voltage-fed (VF) (Figure 1.1) and current-fed (CF) (Figure 1.2) converters, possessing different steady-state and dynamic properties even though the power stage can be the same in both of the cases [7,22]. The term current source has already been widely used, for example, in Ref. [23–28], denoting a voltage-fed converter, where an inductor is placed on the input-side current path such as a boost-type converter [29] or two-inductor (super)buck converter [30]. Fuel cells as renewable energy sources [31] are such an input source, which can be considered to be either voltage or current sources due to their rather constant

Power Electronic Converters: Dynamics and Control in Conventional and Renewable Energy Applications, First Edition. Teuvo Suntio, Tuomas Messo, and Joonas Puukko.

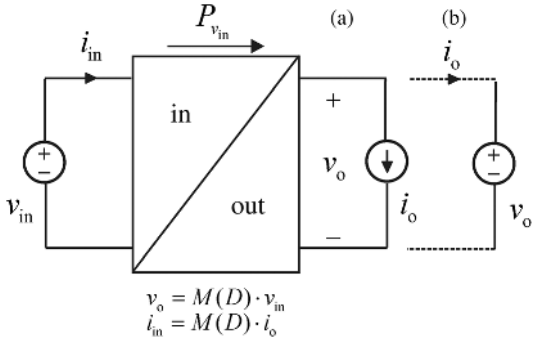

Figure 1.1 VF converter. (a) VO mode. (b) CO mode. *Source*: Suntio 2014. Reproduced with permission of IEEE.

output impedance [32] and operation at the voltages less than the maximum power point [33]. Therefore, the elimination of the harmful low-frequency ripple can be performed by using either input current (i.e., voltage source) or input voltage (i.e., current source) feedback control [34].

On the load side, the output voltage of a converter shall not be taken automatically as an output variable, since this is true only when the converter serves as a typical power supply, regulating its output voltage. In case, the converter is used, for example, as a battery charger or grid-connected inverter, the output voltage is determined by the load-side source and hence output current shall be treated as an output variable. Therefore, the static input-to-output ratio $M(D)$, where D denotes the steady-state duty cycle, shall be actually determined as the ratio of the input-terminal variable characterizing the input source and the same variable at the output terminal, that is, the voltage ratio in a VF converter and the current ratio in a CF converter. According to Figures 1.1 and 1.2, the converter may serve either as a VF or as a CF converter with voltage (VO) or current (CO) as its main output variable, depending on the application. In all the cases, the terminal constraints in terms of voltage and current levels remain unchanged. Reference [22] shows explicitly in theory and by experimental measurements that the dynamic behavior changes significantly application by application as demonstrated in Figure 1.3, where the measured frequency responses of the control-to-output transfer functions with different terminal source configurations are shown. Therefore, it is very important to identify the correct nature of the terminal sources when analyzing the dynamics of the

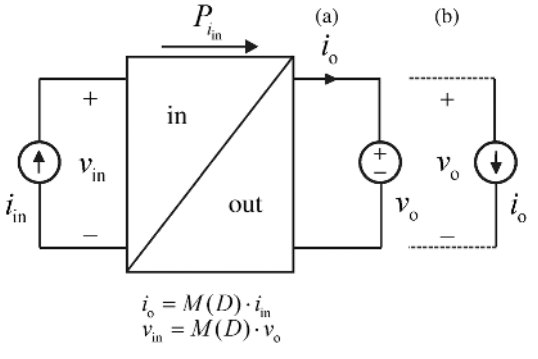

Figure 1.2 CF converter. (a) CO mode. (b) VO mode. *Source*: Suntio 2014. Reproduced with permission of IEEE.

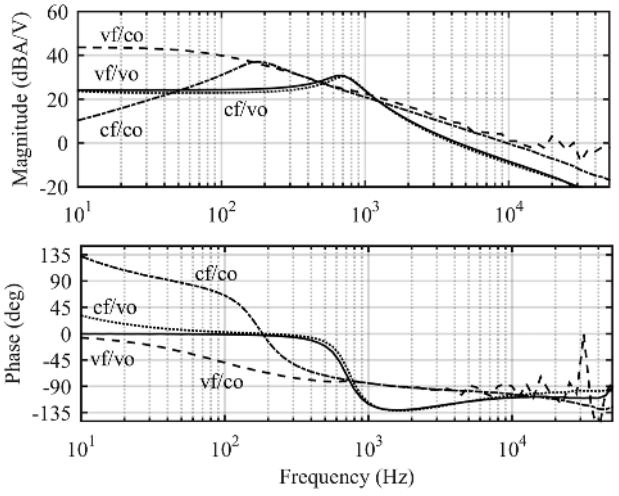

Figure 1.3 The frequency responses of a buck power stage converter when the terminal sources are varied (i.e., voltage-fed converters at voltage (vf/vo) and current (vf/co) output modes and current-fed converters at current (cf/co) and voltage (cf/vo) modes).

converter, for example, for control design purposes, which is obvious when studying the frequency responses in Figure 1.3.

Every power electronic converter has unique internal dynamics, which will determine the obtainable transient dynamics and robustness of stability as well as its sensitivity to the external source and load impedances [35–37]. The internal dynamics can be represented by a certain set or sets of transfer functions, which are classified in circuit theory according to the network parameters [38] known as G (Figure 1.1a), Y (Figure 1.1b), H (Figure 1.2a), and Z (Figure 1.2b), respectively. The specific transfer functions can be directly modeled and measured as frequency responses only when the used terminal sources correspond to the ideal terminal sources given for each of the sets in Figures 1.1 and 1.2. Even if the concept of internal dynamics is basically well known (i.e., all effects from the source and load impedances are removed) [7,35], the tendency is still to use a resistor as a load [39] yielding load-affected models or measured frequency responses. A power stage fed by a certain input source under direct duty ratio (DDR) control tends to maintain the output mode the same as the input source (i.e., VF converters are inherently voltage sources at their output, and CF converters are current sources at their output). As a consequence, the internal transfer functions of such converters can be measured directly at open loop. The other possible output mode does not work at open loop due to violation of Kirchhoff's voltage or current law. The same also applies for the current-mode control, which changes the converter to be a current-output converter [40]. In such a case, the use of resistive load is well justified, but the internal transfer functions have to be computed from the load-affected transfer functions for being useful [7].

A large number of excellent power electronics textbooks are available, such as Refs [5,7,25,39,41–47], which are dedicated to the converters providing either

DC–DC or DC–AC (AC–DC) conversion, or even both. None of these textbooks presents topics that treat the CF converters even if they exist or may even dominate within the specific application area covered in the specific books. The inclusion of the effect of source and load impedances on the converter dynamics is also usually left out by the topics covered in the books even if they are considered very important in practical applications.

The main goal of this book is to provide the missing information in order to complement the other textbooks as well as to present the base for the dynamic analysis of the converters in a general form, which can be utilized with both analytically derived transfer functions and the experimentally measured transfer functions. As a consequence, the potentials of the theoretical work are extended into practice and for the usage of practicing engineers.

The topics covered in the book are briefly discussed and clarified in the subsequent sections in order to familiarize the reader with the secrets of dynamic modeling, analysis, and control designs in both DC-voltage/current source and AC-voltage/current source domains. The mastering of these items requires quite consistent thinking ability as well as flexibility to change from one set of dynamic descriptions to another while moving on.

1.2 Implementation of Current-Fed Converters

There are actually three different methods to implement CF converters: (i) applying capacitive switching cells to construct CF converters [48] similarly as the inductive switching cells are applied, for example, in Refs [1,2], (ii) applying duality transformation methods [49–53], and (iii) adding a capacitor to the input terminal of a VF converter [54] to satisfy the terminal constraints imposed by the input current source [55]. The duality transformation yields CF converters, which retain the main static and dynamic properties characterizing the original VF converter [52]. The adding of a capacitor at the input terminal of a VF converter yields a CF converter having static and dynamic properties resembling the dual of the original converter, that is, a VF buck converter will have characteristics resembling a boost converter and vice versa [54].

As an example, the power stage of a VF buck converter and its dual, that is, the corresponding power stage of a CF buck converter, are given in Figures 1.4 and 1.5. In the original buck converter, the high-side switch S_{HS} conducts during the

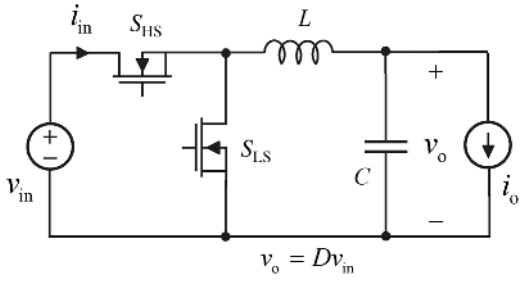

Figure 1.4 VF buck converter.

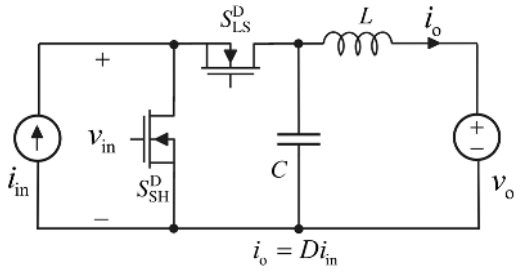

Figure 1.5 CF buck converter.

on-time and the low-side switch S_{LS} during the off-time. In the CF buck converter, the low-side switch S^{D}_{HS} conducts during the on-time and the high-side switch S^{D}_{LS} during the off-time. As both of the converters are buck-type converters, the ideal input-to-output relation or modulo $M(D) = D$.

It has been observed earlier that the VF-converter power stages used in the interfacing of PV generators exhibit peculiar properties, such as appearing of right-half-plane (RHP) zero in the control dynamics of buck power stage converter [56], unstable operation when the output voltage or current is tightly controlled [57], necessity to reduce the pulsewidth for increasing the output variables [58,59], and appearing of RHP pole when peak-current-mode (PCM) control is applied in a buck power-stage converter [60,61], and even the impedance-based stability assessment has to be performed differently compared to the VF converters [62]. The observed phenomena are good evidence for the necessity to fully take into account the used terminal sources as discussed in Ref. [22].

1.3 Dynamic Modeling of Power Electronic Converters

The methods to develop the required small-signal or dynamic models for the power electronic converters date back to the early 1970s [63] when the foundation for the state space averaging (SSA) method was laid down [64] and later modified to correctly capture the dynamics associated with the discontinuous conduction mode (DCM) of operation [65,66] as well as with the variable frequency operation [67,68]. The same methods also apply equally to modeling the dynamics of three-phase grid-connected power converters [69]. The SSA method is observed to produce accurate models up to half the switching frequency.

One of the most fundamental issues in performing the modeling in addition to the recognition of the correct input and output variables is that the state variables are to be considered as the time-varying average values within one switching cycle of the corresponding instantaneous values [66]. In continuous conduction mode (CCM), this is also true in the instantaneous state variables and, therefore, the averaged state space can be constructed by computing the required items directly by applying circuit theory. The continuity is also reflected as the known length of the on-time and off-time. In DCM, the instantaneous variables are not anymore necessarily continuous signals but rather pulsating signals, which is also reflected as the unknown length of off-time. Therefore, their time-varying average values

have to be computed based on the wave shapes of their instantaneous values and used for computing the length of the unknown off-time. A number of variants are available for the basic SSA method in continuous time as well as in discrete time, which can also be used for obtaining the dynamic models but they do not offer usually such benefits, which would justify their usage in practical applications.

The original SSA method can be applied as such only to the converters, which operate in CCM under DDR control, which is also known as voltage-mode (VM) control [39]. The last term is not recommended, however, to be used, because it will mean in the future the internal control methods in a CF converter, where the feedback is taken from the capacitor voltage (i.e., peak voltage mode (PVM) or average voltage mode (AVM)) similarly as the current-mode controls (i.e., peak current (PCM) or average current (ACM)) in a VF converter. The dynamic models (i.e., the small-signal state space) induced by the DDR control will serve as the base for the modeling of the converters, where the internal feedback loops are used to affect the duty ratio generation, that is, the dynamics associated with the duty ratio. The modeling of those converters can be simply done by developing proper duty-ratio constraints, where the perturbed duty ratio is expressed as a function of the state and input variables of the converter [7]. In case of variable-frequency operation, the duty ratio is nonlinear and, therefore, the on-time of the switches has to be used as the control variable instead of duty ratio [7,68].

1.4 Linear Equivalent Circuits

As an outcome of the SSA modeling method [64], the dynamics of the associated converter was represented by means of the canonical equivalent circuit given in Figure 1.6, which is valid for a second-order or two-memory-element converter operating in CCM under DDR control. The structure and the circuit elements of the equivalent circuit can be found from the corresponding small-signal state space. Similar equivalent circuit can also be constructed for the higher order converters as well as for CF converters (see Figure 1.7) applying the same methodology. Figures 1.6 and 1.7 provide clear physical insight into the dynamic processes inside the converters as well as clearly indicate the differences the

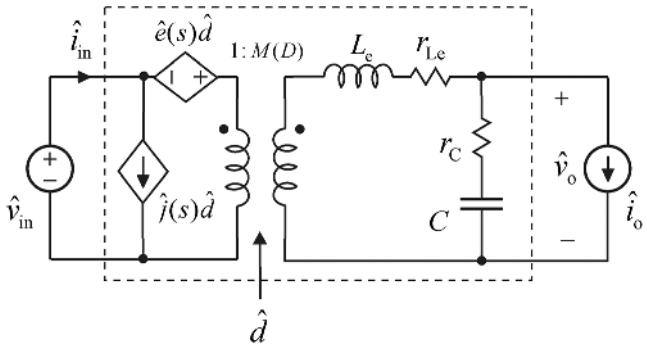

Figure 1.6 Canonical equivalent circuit for a second-order VF/VO converter.

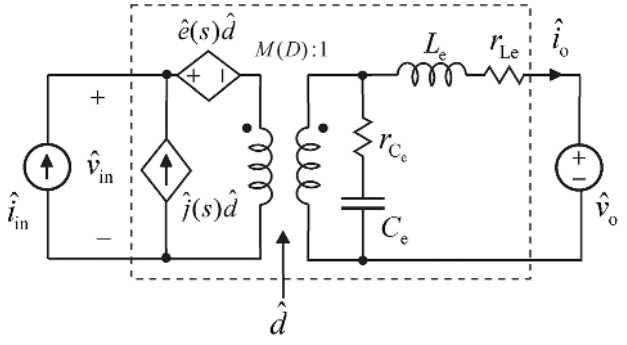

Figure 1.7 Canonical equivalent circuit for a second-order CF/CO converter.

duality transformation produces in the converter. As being a linear representation of the converter, the effect of the source and load impedances can be computed by applying circuit theory, which is very important for understanding the dynamic behavior of the practical systems.

Similar equivalent circuits as in Figures 1.6 and 1.7 cannot be, however, constructed for the converters operating in DCM or containing internal feedbacks, for example, PCM control. More general equivalent circuit can be constructed based on the set of transfer functions comprising the network parameters G, Y, H, and Z, which can be utilized similarly as the canonical equivalent circuits in Figures 1.6 and 1.7 to assess the effect of nonideal source and load [7,70]. Figures 1.8 and 1.9 show such a generic equivalent circuit representing the dynamics of VF/VO DC–DC and a VF/CO DC–DC converters, respectively. On comparing the equivalent circuits in Figures 1.6 and 1.7 with the equivalent circuits in Figures 1.8 and 1.9, the main difference found between them is that the latter equivalent circuits present explicitly the main terminal characteristics of a converter. This information is actually very important for being able to fulfill the terminal constraints stipulated by the different input and output sources.

Similar equivalent circuits as in Figures 1.6 and 1.7 can also be constructed for the three-phase grid-connected converters by means of their small-signal state space given in the synchronous reference frame applying power invariant transformation (i.e., power-invariant d–q state space), as shown in Figures 1.10 and 1.11 [71,72]. The corresponding physical schematics are given in Figures 1.12

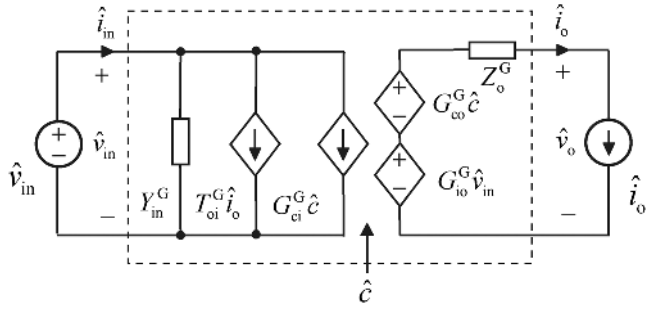

Figure 1.8 Generic equivalent circuit for a VF/VO converter.

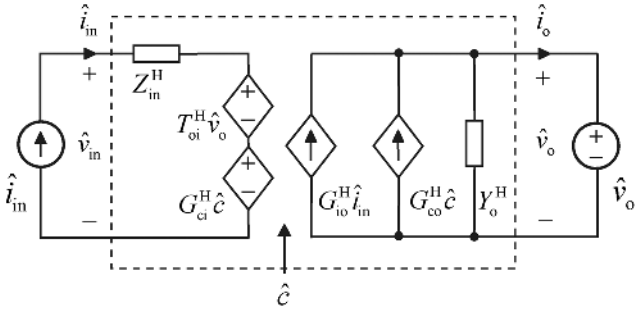

Figure 1.9 Generic equivalent circuit for a CF/CO converter.

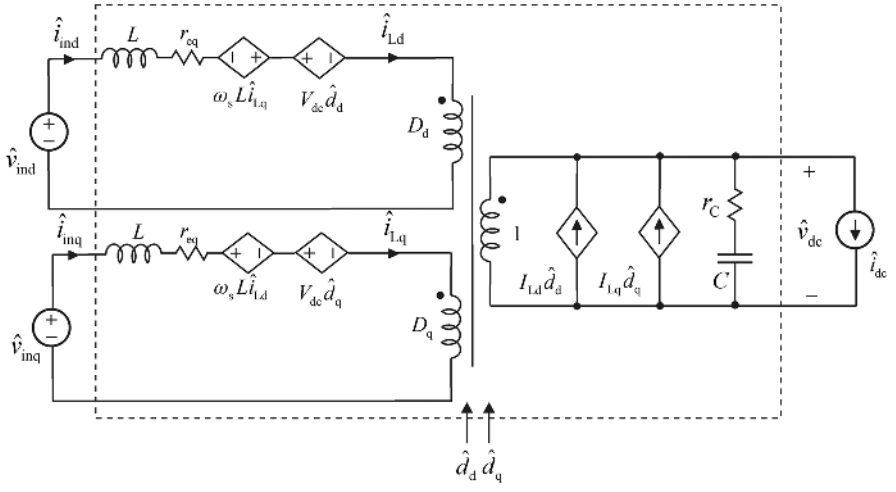

Figure 1.10 Canonical equivalent circuit for a three-phase AC–DC converter.

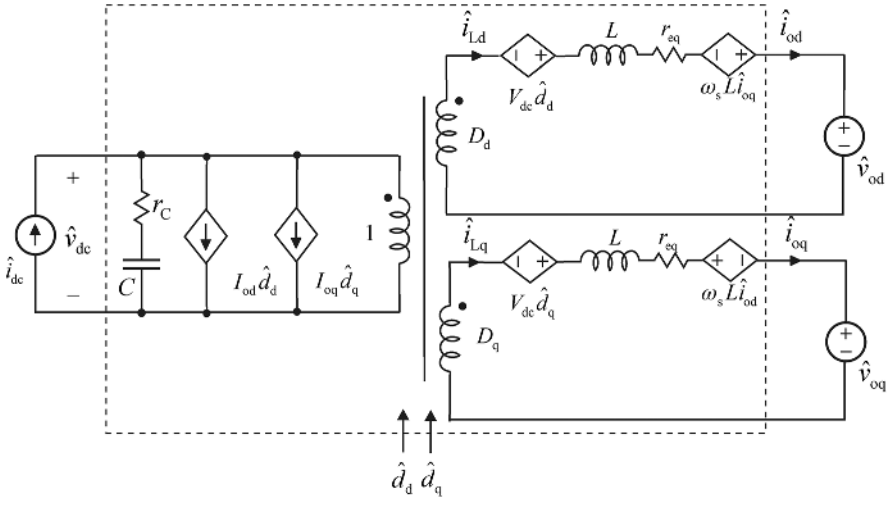

Figure 1.11 Canonical equivalent circuit for a current-fed three-phase DC–AC converter.

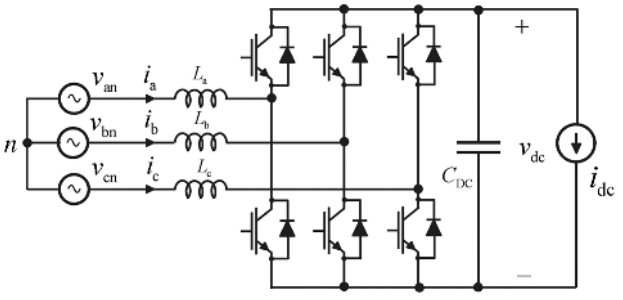

Figure 1.12 Three-phase grid-connected rectifier.

and 1.13, respectively. According to Figures 1.12 and 1.13, the converters can be constructed from each other by changing the direction of power flow. This similarity is also visible in the corresponding equivalent circuits. These equivalent circuits would give the same physical insight as the corresponding DC–DC equivalent circuits.

Similar equivalent circuits as in Figures 1.10 and 1.11 cannot be, however, constructed for the converters operating in DCM or containing internal feedbacks. Similarly, as in the case of DC–DC converters, the more general equivalent circuits can be constructed based on the set of transfer functions comprising the network parameters G, Y, H, and Z, which can be utilized similarly as the canonical equivalent circuits in Figures 1.10 and 1.11 to assess the effect of nonideal source and load [7,73]. Figure 1.14 shows such a generic equivalent circuit representing the dynamics of a three-phase grid-connected AC–DC converter, and Figure 1.15 shows a generic equivalent circuit representing the dynamics of a three-phase grid-connected current-fed inverter. On comparing the equivalent circuits in Figures 1.10 and 1.11 with the equivalent circuits in Figures 1.14 and 1.15, the main difference found between them is that the latter equivalent circuits present explicitly the main terminal characteristics of a converter. This information is actually very important for being able to fulfill the terminal constraints stipulated by the different input and output sources.

The variables of the equivalent circuits with a superscript *s* denote the three-phase variables transformed into the synchronous reference frame (SRF) composed of direct (d) and quadrature (q) components of the variables, respectively. The

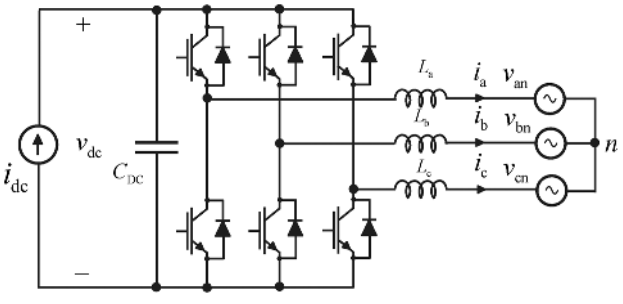

Figure 1.13 Three-phase grid-connected current-fed inverter.

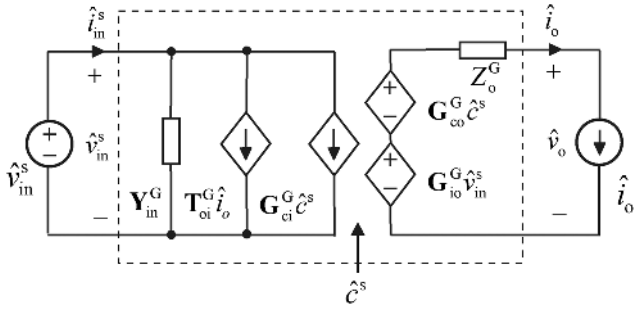

Figure 1.14 Generic equivalent circuit for a three-phase grid-connected VF/VO converter.

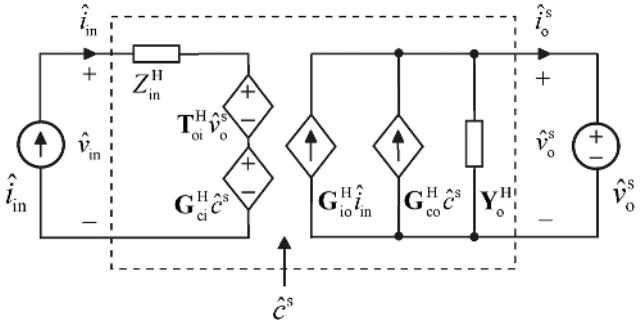

Figure 1.15 Generic equivalent circuit for a three-phase grid-connected CF/CO converter.

transfer functions represented with boldface letters denote a transfer function matrix composed of two or four discrete transfer functions. The computation of the effect of nonideal source and load has to be performed by applying matrix manipulation techniques instead of circuit theoretical methods [73].

The generic equivalent circuits are very flexible tools for solving the dynamic problems associated with the impedance-based interactions [37,71,74] as well as for assessing the stability in the practical interconnected systems [75,76]. The dynamic equivalent circuits as well as the corresponding matrix-form representations can be equally utilized by means of the model-based analytic transfer functions and the corresponding measured frequency responses or even by their combination.

1.5 Impedance-Based Stability Assessment

Stability assessment of a system composed of interconnected power electronic converters as well as passive impedance-like elements can be effectively performed at any interface within the system by means of the ratio of upstream and downstream impedances measured or predicted at the interface [7,22,63,75–84].

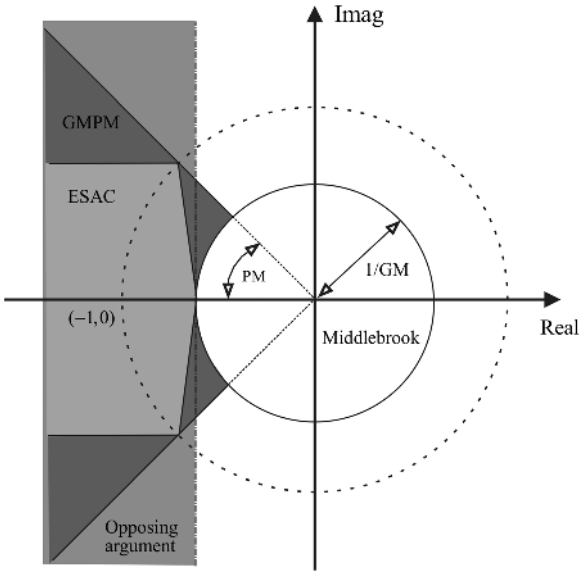

Figure 1.16 Collection of forbidden regions in the complex plane according to Refs [77–84]. *Source*: Vesti 2013. Reproduced with permission of IEEE.

The method was originally launched in Refs [77,78] for designing stable input-filter converter systems. The ratio was named as minor loop gain, where the input-filter output impedance is the upstream impedance and the input impedance of the converter is the downstream impedance. The minor loop gain denotes the ratio of the upstream and downstream impedances. The stability of the interconnected system is retained when the minor loop gain satisfies *Nyquist* stability criterion. It has been later observed that the original minor loop gain is only valid for a certain type of interfaces, that is, the upstream subsystem is a voltage-type system and the downstream system a current-type system. A general definition for the construction of the minor loop gain is such that the numerator impedance shall be the internal impedance of the voltage-type subsystem and the denominator impedance shall be the internal impedance of the current-type subsystem [22,62,78].

The minor loop gain concept is nowadays applied commonly in assessing the stability and transient performance in interconnected power electronic systems. The concept of forbidden region was launched in Ref. [79], which ensures robust stability of the system if the minor loop gain stays out of the forbidden region. The forbidden region launched by Middlebrook in Refs [77,78] is a circle having radius of inverse of gain margin (GM) and the center at origin, as shown in Figure 1.16. Middlebrook's forbidden region was deemed to be too conservative, that is, occupying unnecessary amount of area in the complex plain [79]. As a consequence, new forbidden regions were developed for reducing the conservatism [79–84] such as ESAC (energy systems analysis consortium) [79], GMPM (gain margin phase margin) [80], and opposing argument [81] criteria illustrated in Figure 1.16.

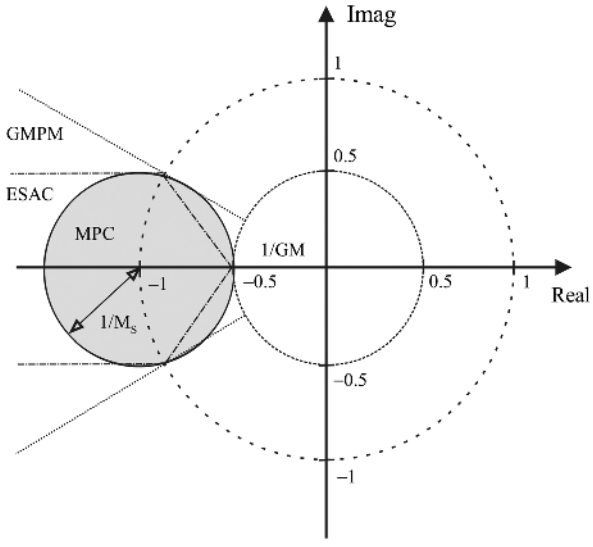

Figure 1.17 Maximum peak criteria (MPC)-based forbidden region versus EASC and GMPM regions [75]. *Source*: Vesti 2013. Reproduced with permission of IEEE.

According to Figure 1.16, all the different criteria aim to maintain robust stability (i.e., acceptable transient performance) by requiring the minor loop gain to satisfy certain PM and GM conditions. Reference [75] proposed a new forbidden region by means of a circle having radius of inverse of maximum peak value allowed in the affected system transfer functions and the center at the point (−1,0) as depicted in Figure 1.17, which outperforms the other earlier launched forbidden regions in terms of occupied area in the complex plain. The forbidden region concept is applicable to DC and AC domain systems as well.

1.6 Time Domain-Based Dynamic Analysis

Time domain-based dynamic analysis and control design are quite common in control engineering [85,86] and are also utilized in conjunction with the grid-connected power electronics applications [87]. The time domain responses do not, however, reveal the origin of the observed transient behavior or how close the system is for instability. Figure 1.18 shows the output-voltage transient behavior of a buck converter when a step change is applied in the load current without (Figure 1.18a) and with the input LC or EMI filters (Figure 1.18b and c). If both the original and EMI filter-affected responses were not known, then it would be very difficult to distinguish between the poor controller design and other external reasons, because the decaying oscillation at the output-voltage response would be similar with low margins (i.e., PM and GM) in the feedback loop.

Figure 1.19 shows the measured output-voltage feedback loop without and with the input EMI filter. According to Figure 1.19, the EMI filter has not caused

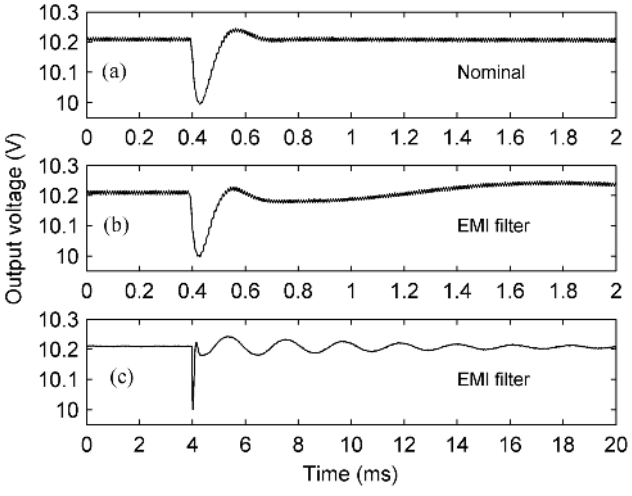

Figure 1.18 Output-voltage response of a buck converter to a step change in load current.

such a change in the feedback loop, which would affect the transient response, that is, the PM and GM are not changed. Figure 1.20 shows the measured closed-loop output impedance of the converter, where the EMI filter has created a resonance, which actually initiates the decaying oscillation at the output-voltage response [88,89]. More specifically, the resonance at the output impedance is caused by the interacting EMI-filter output impedance and short-circuit input impedance of the converter [90].

Figure 1.21 shows that the grid-connected inverter may become unstable when the control bandwidth of the phase locked loop (PLL) is increased under certain grid impedance conditions. PLL is used for synchronizing the inverter to grid. The

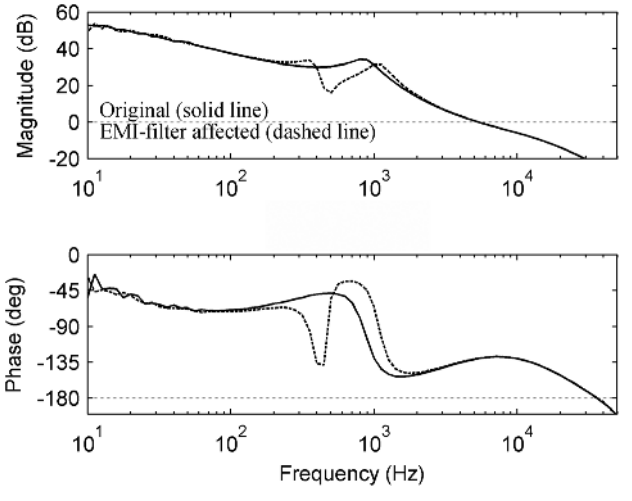

Figure 1.19 The measured original and EMI-filter-affected output-voltage feedback loops.

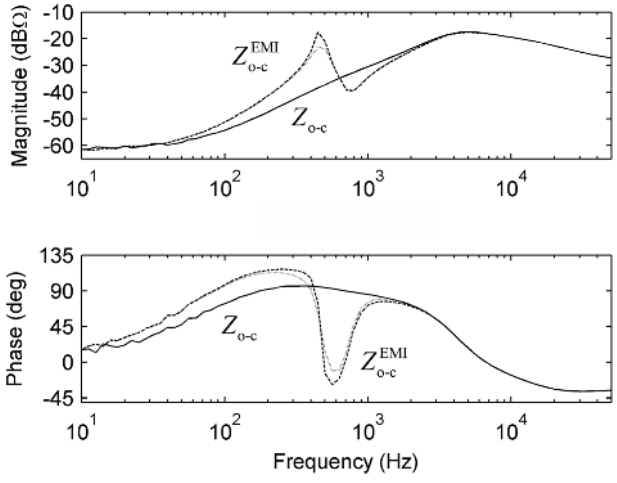

Figure 1.20 Original and EMI-filter-affected closed-loop output impedances.

reason for the instability is the tendency of the inverter output impedance to have negative resistor-like behavior at low frequencies, that is, at the frequencies lower than the PLL crossover frequency [91]. The frequency responses of the inverter output impedance and the grid impedance (Figure 1.22) can be used to reveal explicitly the problems associated with instability phenomenon. The time domain plot does not tell anything about the reasons behind the problem or how much the condition has to change that the instability will vanish or occur again.

It may be quite obvious that the time domain evidence does not suffice to proving the quality of design or the validity of the modifications for removing the problem. The frequency domain evidence will provide a medium to assess the robustness of the design as well as to reveal the risks left in the design for reoccurrence of the "removed" problem.

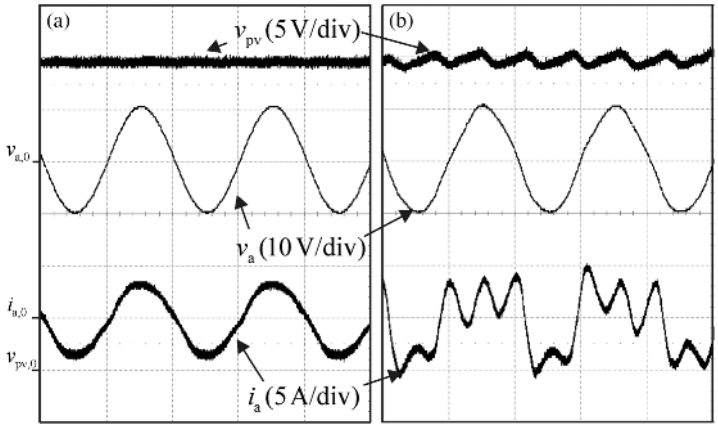

Figure 1.21 Instability of three-phase grid-connected inverter induced by PLL control bandwidth.

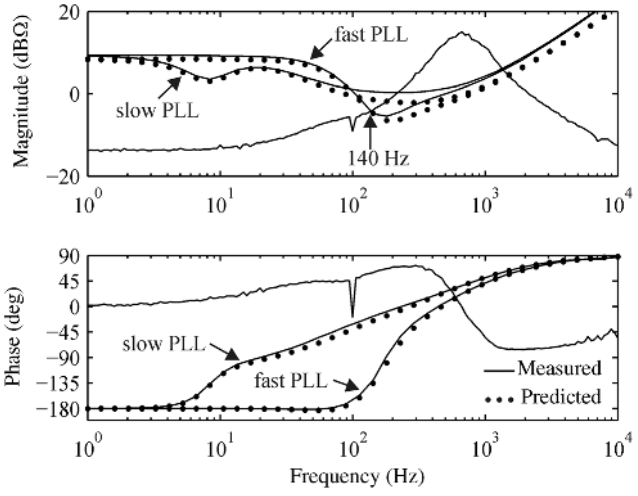

Figure 1.22 Effect of the PLL bandwidth on the inverter output impedance.

1.7 Renewable Energy System Principles

Large-scale utilization of the renewable energy sources such as solar PV, wind, and fuel cells necessitates the use of power electronic converters for providing the grid integration [4]. The solar PV power plants are either constructed by using one DC–AC stage (i.e., single stage) (Figure 1.23) or cascaded by using DC–DC and DC–AC stages (i.e., double stage) (Figure 1.24) [92]. The full-power converter wind energy and fuel cell systems are most often constructed by using double-stage converter schemes according to Figure 1.24 [31,93–95].

The basic operation mode of these systems in terms of grid connection is either grid-parallel (i.e., grid-feeding, grid-supporting) or grid-forming mode [96–98]. In grid-parallel operation mode, the inverter serves as current source, and the grid

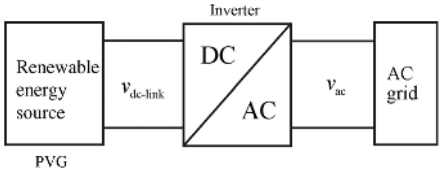

Figure 1.23 Single-stage renewable energy system principle.

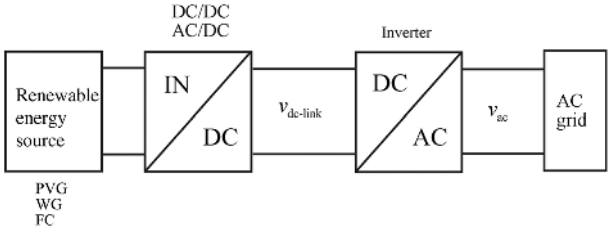

Figure 1.24 Cascaded renewable energy system principle.

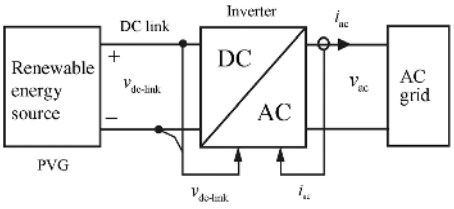

Figure 1.25 Single-stage grid-parallel energy system.

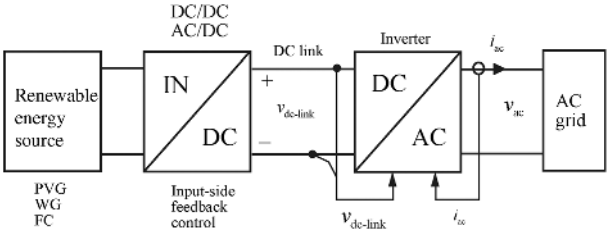

Figure 1.26 Cascaded grid-parallel renewable energy system.

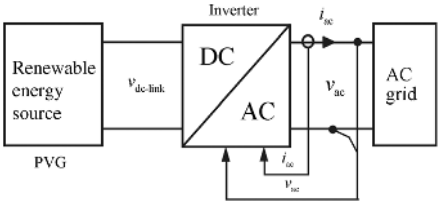

Figure 1.27 Single-stage grid-forming energy system.

determines the level of AC voltage and frequency (Figures 1.25 and 1.26). Usually maximum available power in the renewable energy source is supplied into the grid applying different maximum power point (MPP) tracking algorithms [99–102]. A characteristic of the grid-parallel operation mode is that the outmost feedback loops of the power electronic converters are taken from the input terminal of the converters (see Figures 1.25 and 1.26).

In grid-forming operation mode (i.e., standalone, off-grid, or islanding), the inverter serves as a voltage source taking care of both the voltage level and the frequency (Figures 1.27 and 1.28). The level of output power supplied into the

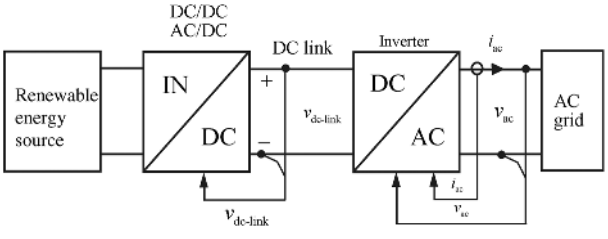

Figure 1.28 Cascaded grid-forming renewable energy system.

system depends on the load of the system. A characteristic of the grid-forming mode is that the outmost feedback loops are taken from the output terminal of the power electronics converters (see Figures 1.27 and 1.28).

The feedback arrangements mean that the power electronic converters in grid-parallel mode are CF/CO converters and in grid-forming mode VF/VO converters. The change of operating mode is usually required in renewable energy systems (i.e., from grid-parallel to grid-forming mode and back). The dynamic behavior of the converters will profoundly change depending on the operation mode, which has to be carefully considered when designing the control systems for ensuring stable operation [97].

1.8 Content Review

The book is divided into four parts as follows: Part One, comprising Chapters 1 and 2, is dedicated to the introduction as well as to the dynamic analysis and control design preliminaries in a generalized manner. Part Two, comprising Chapters 3–6, is dedicated to the dynamics of voltage-fed DC–DC converters. Part Three, comprising Chapters 7–11, is dedicated to the dynamics of current-fed DC–DC converters as well as to the properties of photovoltaic generator and its effects on the interfacing converter dynamics. Part Four, comprising Chapters 12–17, is dedicated to the dynamics and control of grid-connected three-phase VSI-type converters. The content of the subsequent chapters is briefly reviewed in order to clarify the message, which each chapter will deliver.

The conceptual and theoretical basis of the book is provided in Chapter 2 in a simple and practical manner without using difficult mathematical treatments, but at the same time in general form. The same theoretical formulas are repeated in explicit modes in the associated chapters if deemed to be necessary for understanding the message.

In Part Two, the dynamic modeling, analysis, and control of VF converters are treated. Chapter 3 provides the unified dynamic modeling of direct-on-time-controlled converters applied to the basic converters (i.e., buck, boost, and buck–boost) as well as to the superbuck or two-inductor buck converter in the fixed-frequency mode of operation. The dynamic models provided by Chapter 3 are utilized to model the dynamic behavior of the current-mode-controlled converters in Chapter 4. The similarity between PCM and ACM controls is clearly pointed out. The modeling of PCM control is also introduced in case of several simultaneous inductor-current-feedback arrangements as well as when coupled inductors are utilized. The source and load interactions in PCM- and DDR-controlled converters are compared and the origin of the differences is explained. Chapter 5 introduces the modeling of current-output converters based on the models of the VF/VO converters. The source and load interactions as well as impedance-based stability analysis are introduced and compared with the VF/VO converters. Chapter 6 is dedicated for the control design issues in VF converters. The factors affecting the load transient response are explicitly explained, which would facilitate the control design.

In Part Three, the implementation, dynamic modeling, analysis, and control of CF converters are treated. Chapter 7 provides the methods to implement CF

converters applying duality transformation and adding necessary components at the input terminal for satisfying the terminal constraints imposed by the current-type input source. Chapter 8 provides the dynamic models of DDR-controlled basic CF converters implemented by duality-transformation methods or by adding a capacitor at the input terminal of a VF converter. Chapter 9 introduces the dynamic modeling of PCM- and PVM-controlled CF converters. Observed stability problems in conjunction with PCM control applied in PV interfacing converters are explicitly explained. The influence of the PCM and PVM controls in source and load interactions as well as impedance-base stability assessment are explicitly explained. Chapter 10 introduces the characteristics of PV generator as well as the MPP tracking methods and design constraints. Chapter 11 is dedicated to the photovoltaic generator interfacing problematics from the power electronics converter viewpoint, including the PV generator-induced effects on the dynamics of the interfacing converters as well as the associated stability issues.

In Part Four, the dynamic modeling, analysis, and control of grid-connected three-phase VSI-type converters are treated. Chapter 12 provides consistent methods to develop the dynamic models of voltage- and current-fed three-phase PWM inverters in synchronous reference frame (or dq-domain) by utilizing space vector theory. Chapter 13 is dedicated to applying the dynamic models to design the required control functions in an inverter. The effect of different control anomalies caused by the input terminal sources are explicitly treated as well. Chapter 14 introduces reduced-order dynamic modeling of the inverters to relax the high complexity of the inverter dynamics for achieving satisfactory dynamic descriptions applicable for control design. Chapter 15 provides the detailed models for analyzing the closed-loop dynamics of the inverter in multivariable environment. Chapter 16 provides detailed information on the impedance-ratio-based stability assessment methods applying generalized *Nyquist* stability criterion. Chapter 17 is dedicated to the dynamic modeling and control design of three-phase active rectifiers.

References

1 Tymerski, R. and Vorpérian, V. (1986) Generation, classification and analysis of switched-mode DC-to-DC converters by the use of converter cells. Proceedings of the IEEE INTELEC, pp. 181–195.

2 Tymerski, R. and Vorpérian, V. (1988) Generation and classification of PWM DC-to-DC converters. *IEEE Trans. Aerosp. Electron. Syst.*, **24** (6), 743–754.

3 Bose, B.K. (2010) Global warming: energy, environmental pollution, and the impact of power electronics. *IEEE Ind. Electron. Mag.*, **4** (1), 6–17.

4 Blaabjerg, F., Chen, Z., and Kjaer, S.B. (2004) Power electronics as efficient interface in dispersed power generation. *IEEE Trans. Power Electron.*, **19** (5), 1184–1194.

5 Teodorescu, R., Liserre, M., and Rodriquez, P. (2011) *Grid Converters for Photovoltaic and Wind Power Systems*, John Wiley & Sons, Ltd, Chichester, UK.

6 Suntio, T., Puukko, J., Nousiainen, L., Messo, T., and Huusari, J. ((2011)) Change of paradigm in power electronic converters used in renewable energy

applications. Proceedings of the IEEE 33rd International Telecomunications Energy Conference, pp. 1–9.
7 Suntio, T. (2009) *Dynamic Profile of Switched-Mode Converters: Modeling, Analysis and Control*, Wiley-VCH Verlag GmbH, Weinheim, Germany.
8 Lyi, S. and Dougal, R.A. (2002) Dynamic multiphysics model for solar array. *IEEE Trans. Energy Convers.*, **17** (2), 285–294.
9 Nousiainen, L., Puuko, J., Mäki, A., Messo, T., Huusari, J., Jokipii, J., Viinamäki, J., Torres Lobera, D., Valkealahti, S., and Suntio, T. (2013) Photovoltaic generator as an input source for power electronic converters. *IEEE Trans. Power Electron.*, **28** (6), 3028–3038.
10 Suntio, T., Leppäaho, J., Huusari, J., and Nousiainen, L. (2010) Issues on solar-generator interfacing with current-fed MPP-tracking converters. *IEEE Trans. Power Electron.*, **25** (9), 2409–2419.
11 Suntio, T., Huusari, J., and Leppäaho, J. (2010) Issues on solar-generator interfacing with voltage-fed MPP-tracking converters. *Eur. Power Electron. Drives J.*, **20** (3), 40–47.
12 Ali, M.H., Wu, B., and Dougal, R.A. (2010) An overview of SMES applications in power and energy systems. *IEEE Trans. Sustain. Energy*, **1** (1), 38–45.
13 Shmilovitz, D. and Singer, S. (2002) A switched mode converter suitable for superconductive magnetic energy (SMES) systems. Proceedings of the IEEE APEC, pp. 630–634.
14 Suntio, T. (2013) Editorial: special issue on power electronics in photovoltaic applications. *IEEE Trans. Power Electron.*, **28** (6), 2647–2648.
15 Viinamäki, J., Kivimäki, J., Suntio, T., and Hietalahti, L. (2014) Design of boost-power-stage converter for PV generator interfacing. Proceedings of the EPE-ECCE, pp. 1–10.
16 Ho, C., Breuninger, H., Pettersson, S., Escobar, G., Serpa, L.A., and Coccia, A. (2012) Practical design and implementation of an interleaved boost converter using SiC diodes for PV application. *IEEE Trans. Power Electron.*, **27** (6), 2835–2845.
17 Ho, C., Breuninger, H., Pettersson, S., Escobar, G., and Canales, F. (2013) A comparative performance study of an interleaved boots converter using commercial Si and SiC diodes for PV application. *IEEE Trans. Power Electron.*, **28** (1), 289–299.
18 Debonei, H., Lee, S.R., and Nehrir, H. (2009) Direct energy transfer for high efficiency photovoltaic Part I: concepts and hypothesis. *IEEE Trans. Aerosp. Electron. Syst.*, **45** (1), 31–45.
19 Villalva, M.G., de Siqueira, T.G., and Ruppert, E. (2010) Voltage regulation of photovoltaic arrays: small-signal analysis and control design. *IET Power Electron.*, **3** (6), 869–880.
20 Chen, Y.-M., Huang, A.Q., and Yu, X. (2013) A high step-up three-port DC–DC converter for stand-alone PV/battery power systems. *IEEE Trans. Power Electron.*, **28** (11), 5049–5062.
21 Figueros, E., Garcerá, G., Sandia, J., Gonzáles-Espín, F., and Rubio, J.C. (2009) Sensitivity study of the dynamics of three-phase photovoltaic inverters with an LCL grid filter. *IEEE Trans. Ind. Electron.*, **56** (3), 706–717.

22 Suntio, T., Viinamäki, J., Jokipii, J., Messo, T., and Kuperman, A. (2014) Dynamic characteristics of power electronic interfaces. *IEEE J. Emerg. Sel. Top. Power Electron.*, **2** (4), 949–961.

23 Williams, B.W. (2013) DC-to-DC converters with continuous input and output power. *IEEE Trans. Power Electron.*, **28** (5), 2307–2316.

24 Williams, B.W. (2014) Generation and analysis of canonical switching cell DC-to-DC converters. *IEEE Trans. Ind. Electron.*, **61** (1), 329–346.

25 Krein, P. (1998) *Elements of Power Electronics*, Oxford University Press, New York, NY.

26 Sahan, B., Vergara, A.N., Henze, N., Engler, A., and Zacharias, P. (2008) A single-stage PV module integrated converter based on a low-power current-source inverter. *IEEE Trans. Ind. Electron.*, **55** (7), 2602–2609.

27 Wolfs, P.J. (1993) A current-sourced DC–DC converter derived via the duality principle from half-bridge converter. *IEEE Trans. Ind. Electron.*, **40** (1), 139–144.

28 Weaver, W.W. and Krein, P.T. (2007) Analysis and applications of a current-sourced buck converter. Proceedings of the IEEE APEC, pp. 1664–1670.

29 Chen, Y. and Smedley, K. (2008) Three-phase boost-type grid-connected inverter. *IEEE Trans. Power Electron.*, **23** (5), 2301–2309.

30 Karppanen, M., Arminen, J., Suntio, T., Savela, K., and Simola, J. (2008) Dynamical modeling and characterization of peak-current-mode-controlled superbuck converter. *IEEE Trans. Power Electron.*, **23** (3), 1370–1380.

31 Thounthong, P., Davat, B., Raël, S., and Sethakul, P. (2009) Fuel cell high-power applications: an overview of power converters for clean energy conversion technology. *IEEE Ind. Electron. Mag.*, **3** (1), 32–46.

32 Marquezini, D.D., Ramos, D.B., Machado, R.Q., and Farret, F.A. (2008) Interaction between proton exchange membrane fuel cells and power converters for AC integration. *IET Renew. Power Gen.*, **2** (3), 151–161.

33 Giustiniani, A., Petrone, G., Spagnuolo, G., and Vitelli, M. (2010) Low-frequency current oscillations and maximum power point tracking in grid-connected fuel-cell-based systems. *IEEE Trans. Ind. Electron.*, **57** (6), 2042–2053.

34 Gemmen, R.S. (2003) Analysis for the effect of inverter ripple current on fuel cell operating condition. *J. Fluids Eng.*, **125** (3), 576–585.

35 Suntio, T., Hankaniemi, M., and Karppanen, M. (2006) Analysing the dynamics of regulated converters. *IEE Proc. Electric Power Appl.*, **153** (6), 905–910.

36 Hankaniemi, M., Karappanen, M., and Suntio, T. (2006) Load imposed instability and performance degradation in a regulated converter. *IEE Proc. Electric Power Appl.*, **153** (6), 781–786.

37 Vesti, S., Suntio, T., Oliver, J.A., Prieto, R., and Cobos, J.A. (2013) Effect of control method on impedance-based interactions in a buck converter. *IEEE Trans. Power Electron.*, **28** (11), 5311–5322.

38 Tse, C.K. (1998) *Linear Circuit Analysis*, Addison-Wesley, Harlow, UK.

39 Erickson, R.W. and Maksimovic, D. (2001) *Fundamentals of Power Electronics*, Kluwer Academic Publishers, Norwell, MA.

40 Suntio, T., Karppanen, M., and Sippola, M. (2008) Methods to characterize open-loop dynamics of current-mode-controlled converters. Proceedings of the IEEE Power Electron, pp. 636–642.

41 Batarseh, I. (2004) *Power Electronic Circuits*, John Wiley & Sons, Inc., Hoboken, NJ.
42 Choi, B. (2013) *Pulsewidth Modulated DC-to-DC Power Conversion: Circuits, Dynamics, and Control Designs*, John Wiley & Sons, Inc., Hoboken, NJ.
43 Ioinovici, A. (2013) *Power Electronics and Energy Conversion Systems, Volume 1, Fundamentals and Hard-Switching Converters*, John Wiley & Sons, Ltd, Chichester, UK.
44 Kazimierczuk, M.K. (2008) *Pulse-Width Modulated DC–DC Power Converters*, John Wiley & Sons, Ltd, Chichester, UK.
45 Yazdani, A. and Iravani, R. (2010) *Voltage-Sourced Converters in Power Systems*, John Wiley & Sons, Inc., Hoboken, NJ.
46 Bacha, S., Munteanu, I., and Bratcu, A.I. (2014) *Power Electronic Converter Modeling and Control*, Springer, London, UK.
47 Zhong, Q.-C. and Hornik, T. (2013) *Control of Inverters in Renewable Energy and Smart Grid Integration*, John Wiley & Sons, Ltd, Chichester, UK.
48 Shmilovitz, D. (2006) Gyrator realization based on a capacitive switched cell. *IEEE Trans. Circuits Syst. II Express Briefs*, **53** (12), 1418–1422.
49 Desoer, C.A. and Kuh, E.S. (1969) *Basic Circuit Theory*, McGraw-Hill Kogausha, Tokyo, Japan, pp. 444–449.
50 Luenberger, D.G. (1992) A double look at duality. *IEEE Trans. Automat. Contr.*, **37** (10), 1474–1482.
51 Cuk, S. (1979) General topological properties of switching structures. Proceedings of the IEEE PESC, pp. 109–130.
52 Leppäaho, J. and Suntio, T. (2011) Dynamic characteristics of current-fed superbuck converter. *IEEE Trans. Power Electron.*, **26** (1), 200–209.
53 Shmilovitz, D. (2005) Application of duality for deriving of current converter topologies. *HAIT J. Science Eng. B*, **2** (3–4), 529–557.
54 Leppäaho, J., Nousiainen, L., Puukko, J., Huusari, J., and Suntio, T. (2010) Implementing current-fed converters by adding an input capacitor at the input of voltage-fed converter for interfacing solar generator. Proceedings of the EPE-PEMC'10, pp. 81–88.
55 Huusari, J. and Suntio, T. (2012) Interfacing constraints of distributed maximum power point tracking converters in photovoltaic applications. Proceedings of the EPE-PEMC'12, pp. DS3d.1-1–DS31-7.
56 Glass, M.C. (1977) Advancements in the design of solar array to battery charge current regulators. Proceedings of the IEEE PESC, pp. 346–350.
57 Capel, A., Marpinard, J.C., Jalade, J., and Valentin, M. (1983) Current fed and voltage fed switching dc/dc converters: steady state and dynamic models, their applications in space technology, Proceedings of the IEEE INTELEC, pp. 421–430.
58 Kuwabara, K. and Suzuki, T. (1984) A pulse-width controlled dc–dc converter powered by a constant-current source. Proceedings of the IEEE INTELEC, pp. 468–472.
59 Xiao, W., Ozog, N., and Dunford, W.G. (2007) Topology study of photovoltaic interface for maximum power point tracking. *IEEE Trans. Ind. Electron.*, **54** (3), 1696–1704.
60 Siri, K. (2000) Study of system instability in solar-array-based power systems. *IEEE Trans. Aerosp. Electron. Syst.*, **36** (3), 957–964.

61 Leppäaho, J. and Suntio, T. (2014) Characterizing the dynamics of peak-current-mode-controlled buck-power-stage converter in photovoltaic applications. *IEEE Trans. Power Electron.*, **29** (7), 3840–3847.

62 Leppäaho, J., Huusari, J., Nousiainen, L., Puukko, J., and Suntio, T. (2011) Dynamic properties and stability assessment of current-fed converters in photovoltaic applications. *IEEJ Trans. Ind. Appl.*, **131** (8), 976–984.

63 Wester, G.W. and Middlebrook, R.D. (1973) Low-frequency characterization of switched dc–dc converters. *IEEE Trans. Aerosp. Electron. Syst.*, **AES-9** (3), 376–385.

64 Middlebrook, R.D. and Ćuk, S. (1977) A general unified approach to modeling switching-converter power stages. *Int. J. Electron.*, **42** (6), 521–550.

65 Sun, J., Mitchell, D.M., Greuel, M.F., Krein, P.T., and Bass, R.M. (2001) Average modeling of PWM converters in discontinuous modes. *IEEE Trans. Power Electron.*, **16** (4), 482–492.

66 Suntio, T. (2006) Unified average and small-signal modeling of direct-on-time control. *IEEE Trans. Ind. Electron.*, **21** (2), 287–295.

67 Sun, J. (2002) Small-signal modeling of variable-frequency pulsewidth modulators. *IEEE Trans. Aerosp. Electron. Syst.*, **38** (3), 1104–1108.

68 Suntio, T. (2006) Average and small-signal modeling of self-oscillating flyback converter with applied switching delay. *IEEE Trans. Power Electron.*, **21** (2), 479–486.

69 Puukko, J. and Suntio, T. (2012) Dynamic properties of a voltage source inverter-based three-phase inverter in photovoltaic application. *IET Renew. Power Gen.*, **6** (6), 381–391.

70 Maranesi, P.G., Tavazzi, V., and Varoli, V. (1988) Two-port characterization of PWM voltage regulators at low frequencies. *IEEE Trans. Ind. Electron.*, **35** (3), 444–450.

71 Figueres, E., Garcerá, G., Sandia, J., González-Espín, F., and Calvo Rubio, J. (2009) Sensitivity study of the dynamics of three-phase photovoltaic inverters with an LCL grid filter. *IEEE Trans. Ind., Electron.*, **56** (3), 706–717.

72 Cvetkovic, I., Jaksic, M.M., Boroyevich, D., Mattavelli, P., Lee, F.C., Shen, Z., Ahmed, S., and Dong, D. (2011) Un-terminated, low-frequency terminal-behavioral d–q model of three-phase converters. Proceedings of the IEEE ECCE, pp. 791–798.

73 Puukko, J. and Suntio, T. (2012) Modelling the effect of a non-ideal load in three-phase converter dynamics. *IET Electron. Lett.*, **48** (7), 402–404.

74 Messo, T., Jokipii, J., Puukko, J., and Suntio, T. (2014) Determining the value of DC-link capacitance to ensure stable operation of three-phase photovoltaic inverter. *IEEE Trans. Power Electron.*, **29** (2), 665–673.

75 Vesti, S., Suntio, T., Oliver, J.A., Prieto, R., and Cobos, J.A. (2013) Impedance-based stability and transient-performance assessment applying maximum peak criteria. *IEEE Trans. Power Electron.*, **28** (5), 2099–2104.

76 Sun, J. (2011) Impedance-based stability criterion for grid-connected inverters. *IEEE Trans. Power Electron.*, **26** (11), 3075–3078.

77 Middlebrook, R.D. (1976) Input filter considerations in design and applications of switching regulators. Proceedings of the IEEE Industry Applications Society Annual Meeting, pp. 91–107.

78 Middlebrook, R.D. (1978) Design techniques for preventing input-filter oscillations in switched-mode regulators. Proceedings of the Power Conversion Conference, pp. A3.–A3.16.

79 Sudhoff, S.D., Glover, S.F., Lamm, P.T., Schmucker, D.H., and Delisle, D.-E. (2000) Admittance space stability analysis of power electronic systems. *IEEE Trans. Aerosp. Electron. Syst.*, **36** (3), 965–973.

80 Wildrick, C.M., Lee, F.C., Cho, B.H., and Choi, B. (1995) A method for defining the load impedance specifications for a stable distributed power system. *IEEE Trans. Power Electron.*, **10** (3), 280–285.

81 Feng, X., Liu, J., and Lee, F.C. (2002) Impedance specification for stable DC distributed system. *IEEE Trans. Power Electron.*, **17** (2), 157–162.

82 Liu, J., Feng, X., Lee, F.C., and Borojevich, D. (2002) PEBB system stability margin monitoring. *J. Vib. Control*, **8** (2), 261–276.

83 Liu, J., Feng, X., Lee, F.C., and Borojevich, D. (2002) Stability margin monitoring using voltage perturbation for DC distributed power systems. *J. Vib. Control*, **8** (2), 277–288.

84 Liu, J., Feng, X., Lee, F.C., and Borojevich, D. (2003) Stability margin monitoring for distributed power systems via perturbation approaches. *IEEE Trans. Power Electron.*, **18** (6), 1254–1261.

85 Hang, C.C., Åström, K.J., and Ho, W.K. (1991) Refinements of the Ziegler–Nichols tuning formula. *IEE Proc. D*, **138** (2), 11–118.

86 Basilio, J.C. and Matos, S.R. (2002) Design of PI and PID controllers with transient performance specification. *IEEE Trans. Educ.*, **45** (4), 364–370.

87 Peña-Alzola, R., Liserre, M., Blaabjerg, F., Ordonez, M., and Yang, Y. (2014) LCL-filter design for robust active damping in grid-connected converters. *IEEE Trans. Ind. Inform.*, **10** (4), 2192–2203.

88 Suntio, T. and Karppanen, M. (2009) The short-circuit input impedance as a main source of input-filter interactions in a regulated converter. *Eur. Power Electron. Drives J.*, **19** (3), 31–40.

89 Suntio, T. and Kivimäki, J. (2014) Physical insight into the factors affecting the load transient response of a buck converter. Proceedings of the European Conference on Power Electronics and Applications, pp. 1–10.

90 Choi, B. (1997) Step load response of a current-mode-controlled DC-to-DC converter. *IEEE Trans. Aerosp. Electron. Syst.*, **33** (4), 1115–1121.

91 Messo, T., Jokipii, J., Aapro, A., and Suntio, T. (2014) Time and frequency-domain evidence on the instability caused by impedance-based interactions in three-phase inverters. Proceedings of the European Conference on Power Electronics and Applications, pp. 1–9.

92 Blaabjerg, F. and Ma, K. (2013) Future on power electronics for wind turbine systems. *IEEE J. Emerg. Sel. Top. Power Electron.*, **1** (3), 139–152.

93 Blaabjerg, F., Liserre, M., and Ma, K. (2012) Power electronics converters for wind turbine systems. *IEEE Trans. Ind. Appl.*, **48** (2), 708–719.

94 Chen, Z., Guerrero, J.M., and Flaabjerg, F. (2009) A review of the state of the art of power electronics for wind turbines. *IEEE Trans. Power Electron.*, **24** (8), 1859–1875.

95 Romero-Cadaval, E., Spagnuolo, G., Franquelo, L.G., Ramos-Paja, C.-A., Suntio, T., and Xiao, W.-M. (2013) Grid-connected photovoltaic generation plants: components and operation. *IEEE Ind. Electron. Mag.*, **7** (3), 6–20.

96 Vasquez, J.C., Guerrero, J.M., Luna, A., Rodríguez, P., and Teodorescu, R. (2009) Adaptive droop control applied to voltage-source inverters operating in grid-connected and islanding modes. *IEEE Trans. Ind. Electron.*, **56** (10), 4088–4096.

97 Kwon, J., Yoon, S., and Choi, S. (2012) Indirect current control for seamless transfer of three-phase utility interactive inverters. *IEEE Trans. Power Electron.*, **27** (2), 773–781.

98 Serban, E. and Serban, H. (2010) A control strategy for a distributed power generation micro grid applications with voltage- and current-controlled source converter. *IEEE Trans. Power Electron.*, **25** (12), 2981–2992.

99 Blaabjerg, F., Teodorescu, R., Liserre, M., and Timbus, A. (2006) Overview of control and grid synchronization for distributed power generation systems. *IEEE Trans. Ind. Electron.*, **53** (5), 1398–1409.

100 Konstantopoulos, G.C. and Alexadridis, A.T. (2014) Full-scale modeling, control, and analysis of grid-connected wind turbine induction generators with back-to-back AC/DC/AC converters. *IEEE J. Emerg. Sel. Top. Power Electron.*, **2** (4), 739–748.

101 Jain, S. and Agarwal, V. (2007) Comparison of the performance of maximum power point tracking schemes applied to single-stage grid-connected photovoltaic systems. *IET Electr. Power Appl.*, **1** (5), 753–762.

102 Subudhi, B. and Pradhan, R. (2013) A comparative study on maximum power point tracking techniques for photovoltaic power systems. *IEEE Trans. Sustain. Energy*, **4** (1), 89–98.